redin Revista Facultad de Ingeniería, Universidad de Antioquia, No.97, pp. 1-13, Oct-Dec 2020

Calibration of NASGRO equation for mixed-mode loading using experimental and numerical data

Calibración de la ecuación NASGRO para modo mixto de carga utilizando datos experimentales y numéricos

David R. Berrios [1], **Rosendo Franco** [1*], **Francisco Rumiche** [2]

[1]Grupo INACOM/Aula PUCP-CIMNE, Sección Ingeniería Mecánica, Departamento de Ingeniería, Pontificia Universidad Católica del Perú. Av. Universitaria 1801. C. P. 15088. Lima, Perú.
[2]Sección Ingeniería Mecánica, Departamento de Ingeniería, Pontificia Universidad Católica del Perú. Av. Universitaria 1801. C. P. 15088. Lima, Perú.

CITE THIS ARTICLE AS:

D. R. Berrios, R. Franco and F. Rumiche. "Calibration of nasgro equation for mixed-mode loading using experimental and numerical data", *Revista Facultad de Ingeniería Universidad de Antioquia*, no. 97, pp. 1-13, Oct-Dec 2020. [Online]. Available: https://www.doi.org/10.17533/udea.redin.20191258

ARTICLE INFO:

Received: May 13, 2019
Accepted: December 20, 2019
Available online: December 20, 2019

KEYWORDS:

Fatigue crack growth; XFEM; stress intensity factors; high yield-strength steel

Crecimiento de fisuras por fatiga; XFEM; factores de intensidad de tensiones; acero de alta resistencia

ABSTRACT: A procedure to calibrate the NASGRO equation in a high yield-strength steel under mixed-mode loading (I+II) is presented. The calibration consists in obtaining the material parameters known as C, m, p and q. The procedure is based on experimental and numerical results. The experimental tests were used to characterize the material and obtain fatigue crack growth data. For the fatigue tests, tapered double cantilever beam (TDCB) specimens with different maximum load and load ratio values were used. Through the numerical analysis, the stress intensity factors, the crack growth direction and the crack path coordinates were calculated. The numerical analysis was performed using XFEM and the maximum energy release rate criterion. The calibrated model allows predicting the number of load cycles with an RMS value of less than 5%, compared with the experimental results.

RESUMEN: Se presenta un procedimiento para calibrar la ecuación de NASGRO en un acero de alta resistencia bajo modo mixto de carga (I + II). La calibración consiste en obtener los parámetros del material conocidos como C, m, p y q. El procedimiento se basa en resultados experimentales y numéricos. Los ensayos experimentales se utilizaron para caracterizar el material y obtener datos del crecimiento de fisuras por fatiga. Para las pruebas de fatiga se utilizaron probetas tipo doble viga en voladizo con sección variable (TDCB), con diferentes valores de carga máxima y razón de carga. Mediante el análisis numérico se calcularon los factores de intensidad de tensiones, la dirección de propagación y las coordenadas de la trayectoria de la fisura. El análisis numérico se realizó usando XFEM y el criterio de la máxima tasa de liberación de energía. El modelo calibrado permite predecir el número de ciclos de carga con un valor RMS inferior al 5%, en comparación con los resultados experimentales.

1. Introduction

Fatigue crack growth in mechanical elements is the result of localized and permanent microstructural changes due to cyclic loads. In order to study crack growth and general crack paths under cyclic loading conditions in a two-dimensional space, a mixed-mode loading (I + II) must be considered [1]. Several investigations have been conducted to evaluate, numerically and experimentally, crack growth direction and crack growth considering combined mode conditions [2–5]. Other authors investigated the influence of surface tension on mixed mode cracks by finite element method [6]. A review of the different criteria and models to evaluate fatigue crack growth and crack growth direction has been presented [7, 8]. In addition, investigations that combine numerical and experimental approaches have been conducted. For example, the fatigue crack growth in a cracked gear

* Corresponding author: Rosendo Franco
E-mail: rofranco@pucp.edu.pe
ISSN 0120-6230
e-ISSN 2422-2844

DOI: 10.17533/udea.redin.20191258

tooth using the NASGRO model and relationships for mixed mode load was analyzed in [9]. Two types of steels, austenitic X15CrNiSi25-20 and martensitic X20Cr13, were investigated in [10]. The authors compared J-integral values on compact tensile (CT) and single-edge notched bend (SENB) specimens using finite element analysis.

Other investigations were focused on the development of procedures and codes to simulate the fatigue crack growth phenomenon. A program called ADAPCRACK for crack growth simulation in 3D was developed [11]. Some researchers used the XFEM and applied Paris Law to evaluate the crack growth velocity and used the maximum main stress criterion to determine the crack growth direction [12]. In order to determine the crack growth direction, several criteria have been proposed, among them: Maximum Tangential Stress criterion (MTS) [13], Minimum Strain Energy Density criterion (SED) [14] and Maximum Energy Release Ratio (MERR) [15]. In the present study, the MERR criterion will be used. According to this criterion, the propagation direction coincides with that in which the energy release ratio (G), given by Equation 1, maximizes.

$$G_{(\theta)} = \frac{K_{I(\theta)}^2 + K_{II(\theta)}^2}{E} \tag{1}$$

Where $K_{\mathrm{I}(\theta)}$ and $K_{\mathrm{II}(\theta)}$ are the stress intensity factors in mode I and mode II, respectively, as defined by Equations 2 and 3, and E is the Young's modulus.

$$K_{\mathrm{I}(\theta)} = \tfrac{1}{4}\left[3\cos\left(\tfrac{\theta}{2}\right) + \cos\left(\tfrac{3\theta}{2}\right)\right] K_{\mathrm{I}} - \tfrac{3}{4}\left[\sin\left(\tfrac{\theta}{2}\right) + \sin\left(\tfrac{3\theta}{2}\right)\right] K_{\mathrm{II}} \tag{2}$$

$$K_{\mathrm{II}(\theta)} = \tfrac{1}{4}\left[\sin\left(\tfrac{\theta}{2}\right) + \sin\left(\tfrac{3\theta}{2}\right)\right] K_{\mathrm{I}} + \tfrac{1}{4}\left[\cos\left(\tfrac{\theta}{2}\right) + 3\cos\left(\tfrac{3\theta}{2}\right)\right] K_{\mathrm{II}} \tag{3}$$

In terms of fatigue crack growth, four high strength steels with martensitic structure were studied and the results were compared with those obtained in other investigations with similar steels [16]. The authors corroborated that the values of the Paris Law parameters are similar for this type of steels. Furthermore, the influence of specimen size parameters on fatigue crack growth rate was evaluated for an AISI 4340 steel, concluding that specimen thickness and width have no significant influence [17]. An empirical law based on the concepts of Linear Elastic Fracture Mechanics (LEFM), which is very useful for predicting the fatigue crack growth in stage II, was proposed [18]. However, there are approaches to predict the fatigue crack growth rate (da/dN) in the three growing stages, being the NASGRO equation (Equation 4), one of the most commonly used [19–22]. This equation incorporates the effect of fatigue crack closing through the f parameter, defined in [23], which depends on the amplitude of the crack opening due to plasticity effects. It also takes into consideration the effect of the fatigue stress intensity ratio (R), under constant amplitude loads, C, m, p and q are empiric material constants, $\triangle K_{TH}$ is the threshold stress intensity factor range for fatigue crack growth, K_{IC} is fracture toughness and $\triangle K$ is the stress intensity factor range. The factor $[(1-f)/(1-R)]^m$ is also known as velocity factor and takes a value of less than 1 when there is a crack closure mechanism [24]; otherwise, it takes the value of 1.

$$\frac{da}{dN} = C\left[\left(\frac{1-f}{1-R}\right)\Delta K\right]^m \frac{\left(1-\frac{\Delta K_{TH}}{\Delta K}\right)^p}{\left[1-\frac{\Delta K}{(1-R)K_{IC}}\right]^q} \tag{4}$$

There are some criteria to determine an equivalent value of the stress intensity factor range when evaluating crack growth in a component subjected to mixed-mode loading ($\mathrm{I}+\mathrm{II}$). In this investigation, the criteria proposed in [25] (hereafter referred to as Tanaka criterion) and [26] (hereafter referred to as Xiangqiao criterion) will be used. Experimental tests in aluminum thin plates with tilted central cracks, based on [27, 28], were conducted in [25]. The author established an equivalent stress intensity factor range according to Equation 5, where $\triangle K_{\mathrm{I}} = K_{\mathrm{I}max} - K_{\mathrm{I}min}$ and $\triangle K_{\mathrm{II}} = K_{\mathrm{II}max} - K_{\mathrm{II}min}$.

$$\triangle K_{eq} = \left(\triangle {K_{\mathrm{I}}}^4 + 8\triangle {K_{\mathrm{II}}}^4\right)^{0.25} \tag{5}$$

The model proposed in [29] for the case of cyclic loading to predict fatigue crack growth in mixed mode, was extended in [26]. Based on MTS criteria, the authors proposed Equation 6 to determine the equivalent stress intensity factor range.

$$\Delta K_{eq} = \frac{1}{2}\cos\left(\frac{\theta}{2}\right)\left[\Delta K_{\mathrm{I}}(1+\cos\theta) - 3\Delta K_{\mathrm{II}}\sin\theta\right] \tag{6}$$

Being θ the crack growth direction, which in turn is determined as defined in [13] (see Equation 7).

$$\left[K_{\mathrm{I}}\sin\theta + K_{\mathrm{II}}\left(3cos\theta - 1\right)\right] = 0 \tag{7}$$

In this investigation, a numerical and experimental analysis of fatigue crack growth for DIN 1.8721 steel has been conducted. The purpose of the investigation is to obtain C, m, p and q parameters of the NASGRO equation using experimental and numerical data. Taking into account that the closing effects can be neglected in high yield-strength steels, in the present work a velocity factor of 1 is used. In addition, the threshold stress intensity factor range was set as $\triangle K_{TH} = 158MPa\sqrt{mm}$ according to [30]. A microstructural and mechanical characterization of the steel used was performed. For the fatigue experimental study, the use of specimens with a tapered double cantilever beam (TDCB) configuration was explored. These specimens facilitate obtaining long and complex crack paths where mixed-mode loading

conditions are produced. In most of the published studies, usually with CT and CTS specimens, the cracks propagate directly to the deflecting hole, obtaining short paths [5, 31, 32]. TDCB samples were pre-cracked and then a deflecting hole was drilled in dissimilar locations, obtaining different propagation paths. In order to obtain the growth data ($\triangle a_E$, $\triangle N_E$) experimentally, a vibrophore machine and the digital image correlation technique (DIC) were used. For the numerical simulation, an XFEM model was implemented in the ANSYS Mechanical platform, using APDL macros developed by the authors. For the calculation of the crack growth direction, the MERR criterion was used. The stress intensity factors, the crack growth direction and the coordinates of the crack path were determined through numerical analysis. Based on numerical results, the two different criteria mentioned, Tanaka and Xiangqiao, were used to determine the equivalent stress intensity factor. Thus, by combining experimental and numerical results, the NASGRO equation parameters were obtained, as explained in the following sections.

2. Experimental procedures

2.1 Material characterization

The DIN 1.8721 steel is a low alloy steel with a nominal carbon content below 0.3%, with very high resistance to wear and impact, and good workability and weldability. It is commonly used in earth moving equipment components, milling and crushing machines, high throughput dies, cutting edges, and in welded components which require high strength and high toughness, such as pressure vessels. Samples for the different tests were obtained by machining processes from a plate (Bohler steel Chronit T-1 500 DIN 1.8721) with a thickness of 16 mm. The actual chemical composition of the steel was obtained by optical emission spectrometry using a Bruker Magellan Q8 spectrometer. The tensile properties were determined according to ASTM A-370 [33], employing a Zwick Roell Z600 tensile test machine. The steel hardness was obtained performing measurements according to ASTM E-18 [34], with a Tinius Olsen durometer. Fracture toughness testing was conducted according to ASTM E-399 [35], samples pre-cracking was generated with a Zwick Roell Vibrophore Amsler 150 HFP 5100 machine. Then, tensile test to rupture was performed with a Zwick Roell Z250 testing equipment. The steel microstructure was revealed by preparing metallographic samples according to ASTM E3 [36], and by using Nital chemical etching as established in ASTM 407 [37].

2.2 Fatigue testing

The samples for fatigue testing were prepared with a geometry based on the TDCB specimen, modified with a drilled hole, i.e. deflecting hole, in order to induce mixed-mode loading conditions (see Figure 1a). Five 12 mm thick samples with different deflecting hole location were manufactured using the XY global coordinate system as a frame of reference. Pre-cracking and fatigue testing were conducted with a Zwick Roell Vibrophore Amsler 150 HFP 5100 machine. Figure 1b shows an actual picture of one of the samples with the pre-crack.

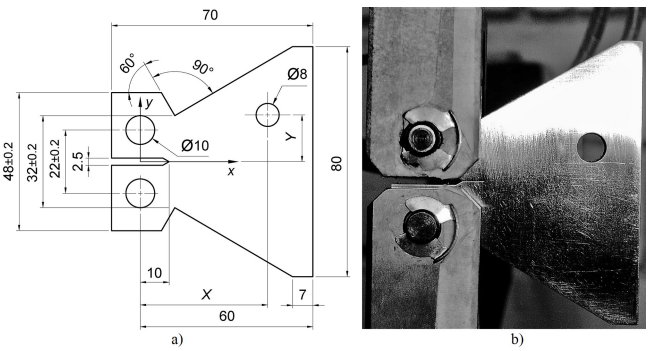

Figure 1 Modified TDCB specimen: a) technical drawing; b) pre-cracked sample picture

The samples parameters for fatigue testing are described in Table 1. The maximum applied load varies between 5 kN and 12 kN, the load ratio R varies between 1/3 and 3/5, each sample is subjected to 2 or 3 load steps. The increase in size crack ($\triangle a_E$), the corresponding number of cycles ($\triangle N_E$), and the crack propagation path, were recorded for each load step.

The crack propagation path was recorded using a commercial DIC system (GOM Aramis). The DIC system was made up of two 1624x1236 pixels resolution optical cameras with 35 mm lens, a measuring distance of 715 mm and a measuring area of 400x300 mm. In order to determine $\triangle a_E$, the obtained images were inserted in a CAD software and the crack size corresponding to each $\triangle N_E$ was measured. $\triangle N_E$ was directly obtained from the Vibrophore machine software. Figure 2 shows the experimental set-up for fatigue testing, including the DIC system.

3. Numerical simulation procedure

The fatigue crack growth simulation was carried out in ANSYS Mechanical APDL. For this purpose, an XFEM model was implemented using algorithms (APDL macros) developed by the authors [38]. A first order quadrilateral mesh was generated with a significant refinement in the zone where crack propagation is predicted to occur (see

Table 1 Samples parameters for fatigue testing

Sample N°	Location of the deflecting hole		Test conditions		
	X (mm)	Y (mm)	Load step	Maximum load (kN)	R
1	40.3	13.5	1	10	2/5
			2	7	3/7
2	45.9	10.4	1	9	1/3
			2	7	3/7
			3	5	3/5
3	45.4	10.2	1	9	1/3
			2	7,5	1/3
			3	6	1/3
4	46.1	9.8	1	12	1/3
			2	9	1/3
			3	6	1/3
5	46	10.2	1	12	1/3
			2	9	1/3
			3	6	1/3

Figure 2 Experimental set-up for fatigue testing

Figure 3a). A mesh sensibility analysis was performed in [38] and it was confirmed that a global element size of 1.0 mm and a refined zone element size of 0.1 mm are appropriate to register accurate path results. Then, a pre-crack with the same characteristics as those obtained experimentally (length and placement) for each sample, was introduced. To define the boundary conditions, additional nodes were created at the fixing holes centers, which were rigidly joined to the portion of each hole that is in contact with the pin. The central node of the lower hole was fixed, while the central node of the upper hole was restricted only in the horizontal direction. The load was applied in vertical direction in the upper hole central node. The model was solved in an iterative process, element by element until reaching the deflecting hole. The values of K_{I} and K_{II} were determined and the MERR criterion was used to calculate the crack growth direction through each finite element. Figure 3b shows a representation of the crack propagation (discontinuous line) across the mesh elements. The crack passes through points P_1, P_2 and P_3. The crack growth direction (θ) is determined in the local coordinate system, which is localized in the crack tip and is aligned with the crack in the last cracked element.

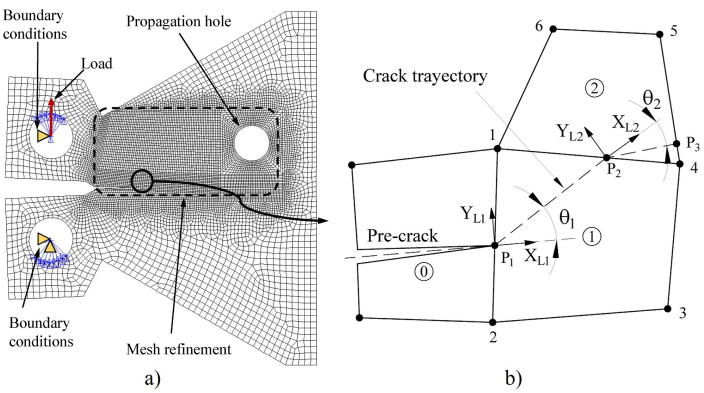

Figure 3 XFEM model: a) mesh and boundary conditions; b) crack representation across the elements

In order to determine the numerical values of K_{I} and K_{II}, the interaction (energy) contour integral method was used [39, 40]. This involves obtaining K_{I} and K_{II} numerical values for several contours. In a similar way to what was proposed in [41], a preliminary value of K_{I} was determined as an average of all contours values without considering the first two, since they are too close to the crack tip. Then, the final value of K_{I}, used in the calculation of the crack growth direction, was set as the one corresponding to the contour with closest value to the average value. The value of K_{II} was obtained from this same contour. Further details about the implemented algorithms, K_{I} and K_{II} calculation, and crack growth direction calculation, are described in another article [38].

The numerical results obtained for each cracked element are registered as indicated in Table 2. The values of K_{I}

and K_{II} in the table represent the maximum values, which correspond to the maximum applied load. To determine the values of $\triangle K_{\mathrm{I}}$ and $\triangle K_{\mathrm{II}}$, the load ratio was used, as shown in Equation 8.

$$\triangle K_{\mathrm{I,II}} = (1 - R)\, K_{\mathrm{I,II}} \tag{8}$$

4. Mathematical model calibration procedure

The objective of the calibration is to determine the values for the NASGRO equation parameters (C, m, p and q) that guarantee the best approximation of calculated results in comparison with those obtained experimentally.

Information that allows estimating the ranges of analyzed parameters values has been found. According to [16], for high yield-strength steels, the C parameter value is in the range of $2.34 \times 10^{-11} \leq C \leq 5.72 \times 10^{-}11$ (using $\triangle a$ in mm and $\triangle K$ in $\mathrm{MPa}\sqrt{mm}$) and the m parameter value is in the range of $2.13 \leq m \leq 2.54$. Furthermore, the p and q parameters values are in the range of $0 \leq p, q \leq 1$, as indicated in [19]. The trial and error method has been used to determine the values of p and q, adjusting to the fatigue crack growth curve [42, 43]. In these investigations, the aluminum 2024-T351 was analyzed, obtaining $p = q = 0$.

The procedure for calibrating the mathematical model is based on the experimental testing and numerical analysis results, as previously described. The procedure consists of the following steps:

1. Calculation of the equivalent stress intensity factor $\triangle K_{eq}$. The numerical results are used to evaluate the two criteria defined by Equations 5 and 6.

2. Definition of the preliminary values of the parameters (C, m, p and q), in the recommended ranges, to perform an initial search. The following values were defined:

   C = (2.20; 2.60; 3.00; 3.40; 3.80; 4.20; 4.60; 5.00; 5.40; 5.80)$\times 10^{-11}$

   m = (2.00; 2.25; 2.5)

   p = (0; 0.25; 0.5; 0.75; 1)

   q = (0; 0.25; 0.5; 0.75; 1)

   All possible combinations with these values are analyzed, with a total number of 750 combinations per sample.

3. Application of the NASGRO equation to calculate the number of cycles according to Equation 9:

$$\Delta N_C = \Delta a \frac{\left[1 - \frac{\Delta K_{eq}}{(1-R)K_{IC}}\right]^q}{C\left(\Delta K_{eq}\right)^m \left(1 - \frac{\Delta K_{TH}}{\Delta K_{eq}}\right)^p} \tag{9}$$

   Where $\triangle N_c$ is the number of cycles calculated for the crack growth $\triangle a$ through the corresponding finite element.

4. Obtaining of the optimal values for the parameters (C, m, p and q).

   - Calculation of the number of cycles error for each sample and all combinations, according to Equation 10:

$$error = 100 \times \frac{N_{CT} - N_{ET}}{N_{ET}} \tag{10}$$

     Where N_{ET} is the total number of cycles obtained experimentally and N_{CT} is the total number of cycles calculated.

     $N_{ET} = \sum_i^j \triangle N_{Ei}$, j is the number of steps ($j = 2$ for sample 1 and $j = 3$ for other samples).

     $N_{CT} = \sum_i^k \triangle N_{Ci}$, k is the total number of cracked finite elements.

   - RMS calculation of the error considering all the 5 samples and all combinations, according to Equation 11:

$$RMS_{\text{error}} = \sqrt{\frac{\sum_{i=1}^{5} \text{error}_i^2}{5}} \tag{11}$$

   - The optimal values for the parameters (C, m, p and q) are defined by the combination in which RMS_{error} value is minimum.

5. Definition of the final values of the parameters (C, m, p and q), refining the ranges from the optimal values (op) obtained in the preliminary analysis. The following values were established:

   $C = (C_{op} \pm 0.25) \times 10^{-11}$, 11 values are taken uniformly distributed within this range.

   $m = m_{op} \pm 0.05$, 5 values are taken uniformly distributed within this range.

   $p = p_{op} \pm 0.05$, 5 values are taken uniformly distributed within this range.

   $q = q_{op} \pm 0.05$, 5 values are taken uniformly distributed within this range.

   In a similar way, as in the preliminary analysis, all possible combinations with these values are analyzed, with a total number of 1375 combinations per sample.

6. To obtain the calibrated values of the parameters (C, m, p and q), steps 3 and 4 of this procedure must be executed again.

Table 2 Numerical results registration template

Cracked finite element	Crack starting coordinates (mm)		Stress intensity factors ($\mathrm{MPa}\sqrt{mm}$)		Crack growth direction	Crack ending coordinates (mm)		Crack length (mm)	Stress intensity factors range $\mathrm{MPa}\sqrt{mm}$	
1	x_1	y_1	$K_{\mathrm{I}1}$	$K_{\mathrm{II}1}$	θ_1	x_2	y_2	$\triangle a_1$	$\triangle K_{\mathrm{I}1}$	$\triangle K_{\mathrm{II}1}$
2	x_2	y_2	$K_{\mathrm{I}2}$	$K_{\mathrm{II}2}$	θ_2	x_3	y_3	$\triangle a_2$	$\triangle K_{\mathrm{I}2}$	$\triangle K_{\mathrm{II}2}$
3	x_3	y_3	$K_{\mathrm{I}3}$	$K_{\mathrm{II}3}$	θ_3	x_4	y_4	$\triangle a_3$	$\triangle K_{\mathrm{I}3}$	$\triangle K_{\mathrm{II}3}$
⋮	⋮	⋮	⋮	⋮	⋮	⋮	⋮	⋮	⋮	⋮
n	x_n	y_n	$K_{\mathrm{I}n}$	$K_{\mathrm{II}n}$	θ_n	x_{n+1}	y_{n+1}	$\triangle a_n$	$\triangle K_{\mathrm{I}n}$	$\triangle K_{\mathrm{II}n}$

Table 3 Chemical composition of the steel DIN 1.8721

C	Si	Mn	P	S	Cr	Mo	Ni	Al
0.211	0.367	0.819	0.0161	0.0007	0.316	0.028	0.112	0.062

5. Results and discussion

5.1 Material properties

Table 3 shows the chemical composition of the steel obtained using Optical Emission Spectroscopy and conforms to the designation DIN 1.8721 for a low alloy steel.

Figures 4a and 4b presents a representative stress-strain curve obtained for a tensile test sample and a picture of the microstructure of the tested steel, correspondingly. The average tensile strength and yield strength were determined to be 1598 MPa and 1480 MPa, respectively. The average Young's modulus was 206 GPa. The microstructure was fully composed of tempered martensite. The average hardness value obtained was 52 HRC. The fracture toughness was calculated to be 3194 $\mathrm{MPa}\sqrt{mm}$. The measured mechanical properties and the observed microstructure are in agreement with a DIN 1.8721 low alloy steel in the quenched and tempered state.

Figures 5a to 5c show images of the fracture surface of toughness test samples with different magnifications, obtained with a Quanta 650-FEI Scanning Electron Microscope (SEM). A mixed fracture pattern with dimples and cleavage is observed in the fracture surface. This mixed fracture pattern is typical in high strength steels. The presence of circular dimples indicates the loading mode I predominance, according to ASTM E-399 [35].

5.2 Fatigue crack growth – Experimental results

Figure 6 shows the crack path experimentally obtained in each sample after the fatigue test. The pre-crack (PC) as well as the crack growth by loading step ($\triangle a_{Ei}$) are labeled for each sample. The crack propagates towards the deflecting hole in all samples, but some differences are observed in the crack path due to small deviations of the pre-crack and different hole locations.

Table 4 shows the experimental results in terms of total crack growth a_{ET} and corresponding total number of cycles N_{ET} for each sample. The total number of cycles (N_{ET}) is calculated as indicated in the step 4 of the mathematical model calibration procedure (section 4). In a similar way, the total crack growth is determined by Equation 12.

$$a_{ET} = \sum_{i}^{j} \Delta a E_i \tag{12}$$

It can be observed that the total number of cycles differs for each sample. This difference occurs due to the different test conditions for each sample, i.e. number of steps, load ratio and maximum load. Samples 1, 2, and 3 show a higher number of cycles than samples 4 and 5, because they have lower maximum load values. In particular, sample 2 exhibited the highest number of cycles (431871), since this sample was subjected to higher values of load ratio. Samples 4 and 5 had similar test conditions, therefore, they have similar values of number of cycles (201827 and 203206, respectively).

5.3 Fatigue crack growth – Numerical results

Table 5 shows part of the numerical results according to the developed template (see Table 2). These results correspond to the optimal combination of the preliminary analysis in sample 1. Although it is a small part of the results, it can be seen that K_{II} presents predominantly negative values and, consistently, θ presents positive values, which means that the crack path is increasing. This trend is similar for most of the crack path in all samples (see Figure 7). In samples 2, 3 and 4, the crack path has

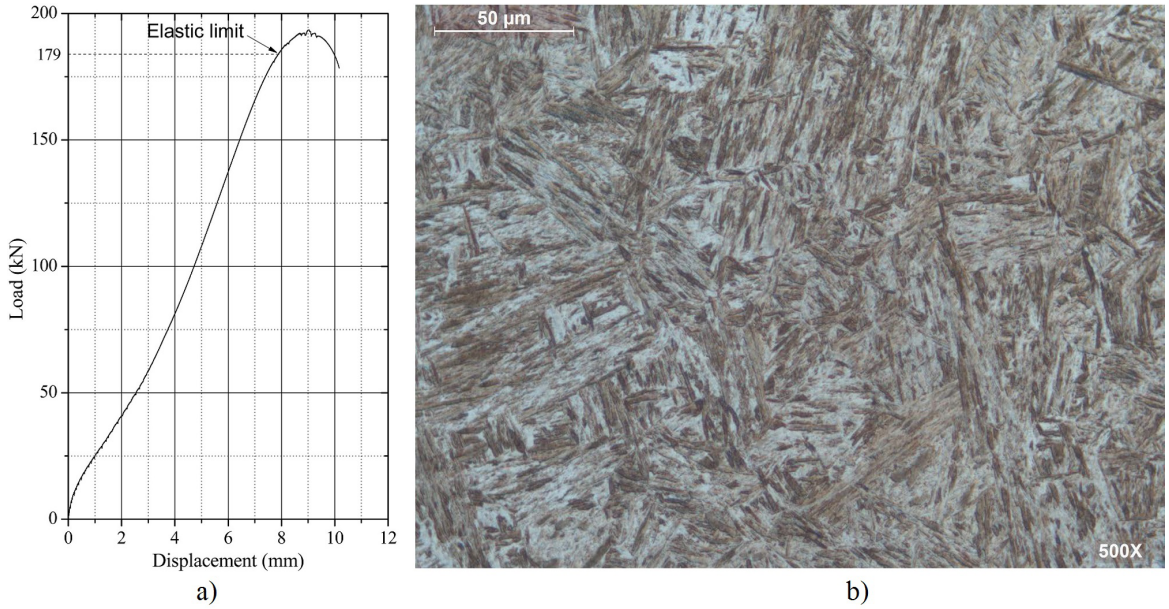

Figure 4 Tested steel characteristics: a) stress-strain curve obtained from tensile test; b) microstructure

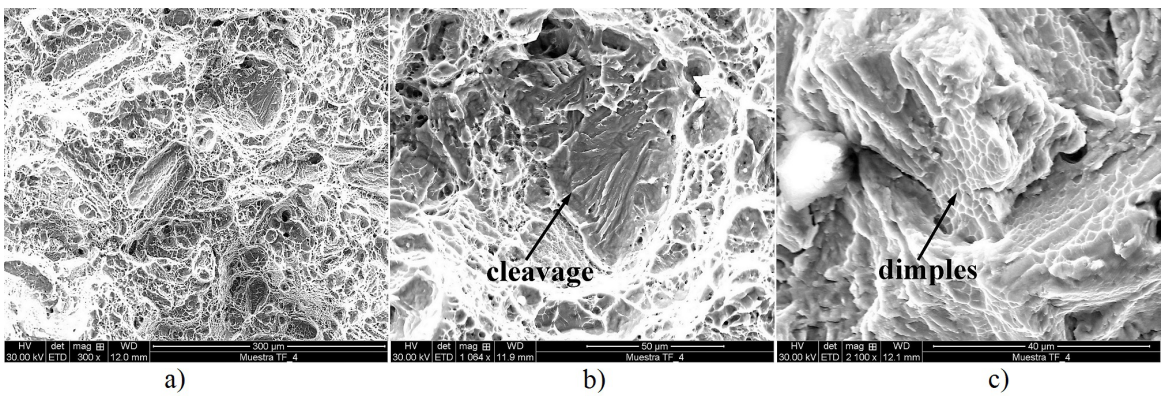

Figure 5 SEM images of the fracture surface from the toughness test samples: a) 300X magnification; b) 1064X magnification; c) 2100X magnification

Table 4 Experimental results of fatigue crack growth

Samples	$\triangle a_{E1}$ (mm)	$\triangle a_{E2}$ (mm)	$\triangle a_{E3}$ (mm)	a_{ET} (mm)	N_{ET} (mm)
1	15	6.6	-	21.6	293971
2	15	8	3	26	431871
3	16	10	3.5	29.5	302727
4	12.6	11.7	2.6	26.9	201827
5	12.5	11.4	2.2	26.1	203206

a small tendency to decrease, so the sign of θ changes to negative.

5.4 Comparison between numerical and experimental results

A quantitative comparison between numerical and experimental results in terms of the total crack growth is presented in Table 6. The absolute error is very small, less than 1% in all samples, with the exception of sample 4 whose absolute error is 2.6%. In this table, the total crack growth is determined by Equation 13.

$$a_{CT} = \sum_{i}^{k} \triangle a_i \tag{13}$$

Figure 7 presents an overlap of the fatigue crack paths

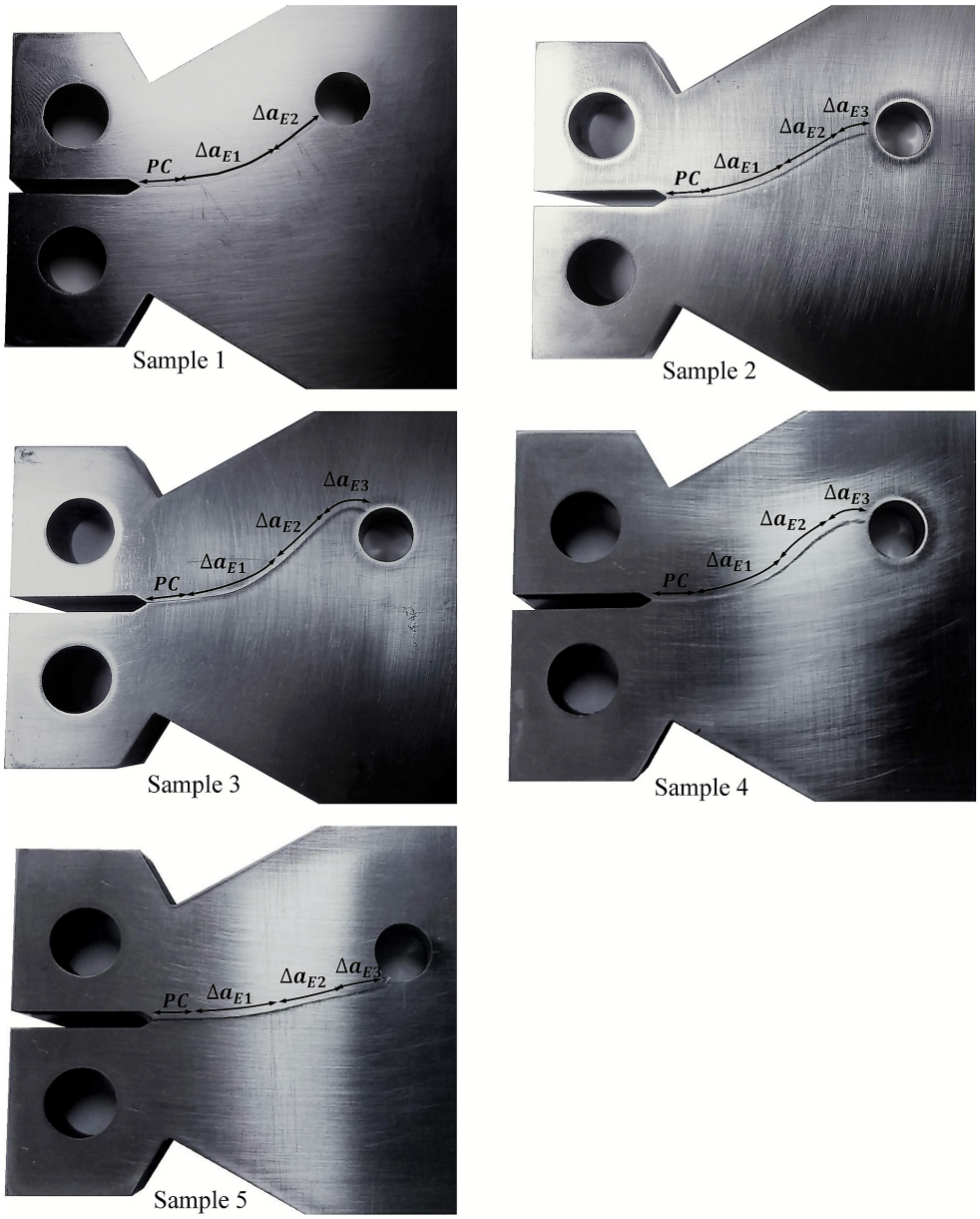

Figure 6 Pre-crack and propagation steps in all samples (1 to 5)

obtained experimentally (continuous red line) and those obtained by numerical simulation (dashed black line). These paths have been plotted in the global coordinate system indicated in Figure 1a. Each path includes the pre-crack (approximately 8 mm length) and the propagation path to the deflecting hole. It can be appreciated that there is a good correlation between numerical and experimental results. The best fit was obtained for samples 1 and 3, with R^2 correlation coefficients of 0.9928 and 0.9970 respectively. The smaller correlation coefficient was obtained for samples 2 and 4, with correlation coefficients of 0.9428 and 0.9552 respectively. The difference may be caused by microstructural defects of the material, such as inclusions, grain boundaries and sliding planes, which could randomly deflect the crack propagation path [44, 45].

5.5 Mathematical model calibration

The numerical results are post-processed to determine $\triangle K_{eq}$ through Tanaka and Xiangqiao criteria, according to developed calibration procedure. Then, the number of cycles to crack each finite element is calculated using Equation 9. In Table 7, a portion of obtained results is shown, including the studied parameters (C, m, p and q), which values are changed according to the defined combinations. The results shown correspond to the optimal combination of the preliminary analysis for

Table 5 Typical numerical results of fatigue crack growth (Sample 1)

Element	x_1 (mm)	y_1 (mm)	K_{I} $(\mathrm{MPa}\sqrt{mm})$	K_{II}	θ (°)	x_2 (mm)	y_2 (mm)	$\triangle a$ (mm)	$\triangle K_{\mathrm{I}}$ $(\mathrm{MPa}\sqrt{mm})$	$\triangle K_{\mathrm{II}}$
1	18.00	0.31	926.38	-7.39	0.91	18.11	0.32	0.11	555.83	-4.44
2	18.11	0.32	927.89	-5.71	0.71	18.22	0.33	0.11	556.73	-3.43
3	18.22	0.33	929.26	-1.37	0.17	18.30	0.34	0.07	557.56	-0.82
4	18.30	0.34	931.15	-0.51	0.06	18.33	0.34	0.04	558.69	-0.31
5	18.33	0.34	930.67	-1.94	0.24	18.44	0.35	0.11	558.40	-1.16
6	18.44	0.35	931.78	-0.57	0.07	18.55	0.36	0.11	559.07	-0.34
7	18.55	0.36	932.98	-2.50	0.31	18.67	0.37	0.11	559.79	-1.50
8	18.67	0.37	934.12	1.73	-0.21	18.78	0.38	0.11	560.47	1.04
9	18.78	0.38	935.02	-0.02	0.00	18.89	0.40	0.11	561.01	-0.01
10	18.89	0.40	935.98	-0.19	0.02	18.92	0.40	0.03	561.59	-0.11
⋮	⋮	⋮	⋮	⋮	⋮	⋮	⋮	⋮	⋮	⋮
242	35.90	9.18	1670.5	-2.84	0.19	36.02	9.29	0.16	954.58	-1.62

Table 6 Comparison between numerical and experimental results

Samples	a_{ET} (mm)	a_{CT} (mm)	error(%)
1	21.6	21.8	0.93
2	26	25.8	-0.77
3	29.5	29.6	0.34
4	26.9	26.2	-2.60
5	26.1	26.3	0.77

sample 1. It can be observed that the results of $\triangle K_{eq}$ are practically identical for the two used criteria. Therefore, the results of $\triangle N_c$ are the same according to both criteria.

For each sample, the total number of cycles (N_{CT}) is calculated as indicated in the step 4 of mathematical model calibration procedure (Section 4). Table 8 shows this value for the optimal combination of the preliminary analysis in sample 1, as well as the absolute error according to Tanaka and Xiangqiao criteria. For this sample, the absolute error is small (2.15%), but is greater for the other samples.

The results of the preliminary analysis yielded the following optimal values of the parameters under study: $C_{op} = 3.0 \times 10^{-11}$, $m_{op} = 2.25$, $p_{op} = 0$ and $q_{op} = 0$. According to the established procedure, the values considered for the final analysis were:

C = (2.75; 2.80; 2.85; 2.90; 2.85; 3.00; 3.05; 3.10; 3.15; 3.20; 3.25)$\times 10^{-11}$

m = (2.15; 2.20; 2.25; 2.3; 2.35)

p = (0; 0,025; 0.05; 0.075, 0.10)

q = (0; 0,025; 0.05)

Table 9 summarizes the results of the preliminary and final calculations of the parameters C, m, p and q, as well as the absolute error of the calculations with respect to the experiments and the corresponding RMS value. It is observed that the absolute error is lower in some samples from the preliminary analysis compared to the final analysis; however, in correspondence with the optimization criterion used, the RMS is lower in the final analysis. As already mentioned, the results using the two criteria to determine the equivalent stress intensity factor are the same.

It is important to mention that the optimum value of C obtained with the proposed procedure is within the range established experimentally in [16] for high yield-strength steels, while the optimal value of m coincides with that suggested by the same author. On the other hand, the optimal values of p and q are equal to zero, because the experimental data used for calibrating the model are in the stage II of the fatigue crack growth.

Finally, Table 10 presents a comparison between calibrated model and experimental results in terms of the number of cycles. There is a good correlation between calculated and experimental results, with an absolute error in the range of 1.91% to 6.34%.

6. Conclusions

A procedure to calibrate the NASGRO equation using experimental and numerical data has been proposed. The procedure is particularly useful when the experimental values of C and m are not available. If the values of C and m are known, the procedure would be equally useful for determining p and q. The procedure validity has been demonstrated since the optimal values found for C (2.95E-11) and m (2.25) are in correspondence with those obtained experimentally by other authors. This investigation proposes using numerical simulation,

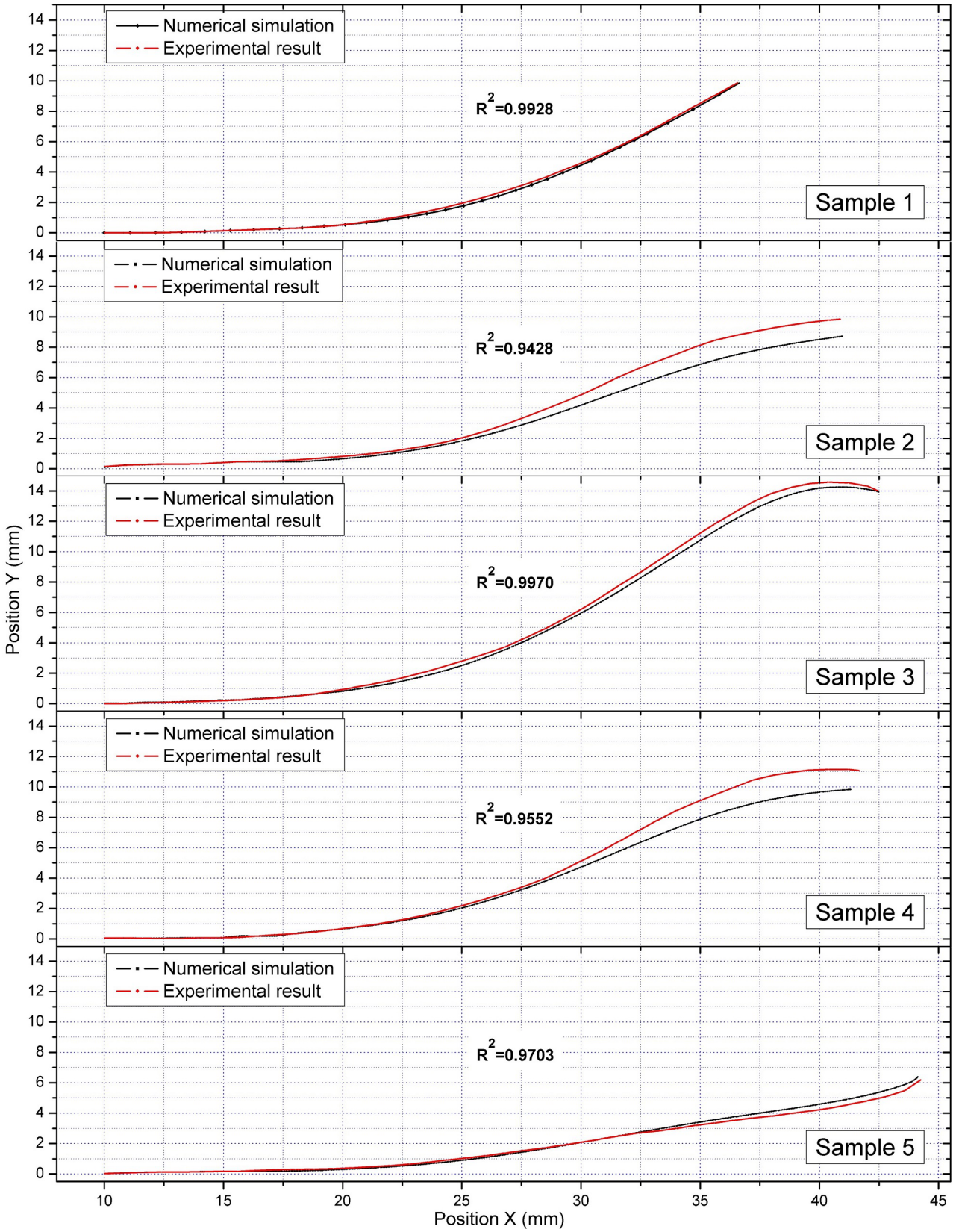

Figure 7 Fatigue crack paths: experimental and numerical results

Table 7 Post-processed results (Sample 1)

$C = 3 \times 10^{-11}$	$p = 0$	$K_{\mathrm{IC}} = 3194\mathrm{MPa}\sqrt{mm}$	
$m = 2.25$	$q = 0$	$\triangle K_{TH} = 158\mathrm{MPa}\sqrt{mm}$	
$\triangle K_{eq} = 158\mathrm{MPa}\sqrt{mm}$		$\triangle N_c$ (cycles)	
Element	**Tanaka**	**Xiangqiao**	**Tanaka**	**Xiangqiao**
1	555.83	555.88	2465.09	2465.09
2	556.73	556.77	2460.43	2460.43
3	557.56	557.56	1614.89	1614.89
4	558.69	558.69	834.41	834.41
5	558.40	558.41	2446.27	2446.27
6	559.07	559.07	2439.75	2439.75
7	559.79	559.80	2434.43	2434.43
8	560.47	560.47	2425.69	2425.69
9	561.01	561.01	2419.89	2419.89
10	561.59	561.59	662.12	662.12
⋮	⋮	⋮	⋮	⋮
242	954.58	954.58	1074.25	1074.25

Table 8 Calculated fatigue crack growth results

	Tanaka	**error (%)**	**Xiangqiao**	**error (%)**
N_{CT} (cycles)	300286.7	2.15	300286.7	2.15

Table 9 Parameters optimal values, absolute error and RMS results

Criteria	**Analysis**	C	m	p	q	**P1 error (%)**	**P2 error (%)**	**P3 error (%)**	**P4 error (%)**	**P5 error (%)**	**RMS (%)**
Tanaka	Preliminary	3.00E-11	2.25	0	0	2.15	-7.90	3.36	-3.96	-3.55	4.62
	Final	2.95E-11	2.25	0	0	3.88	-6.34	5.12	-2.33	-1.91	4.25
Xiangqiao	Preliminary	3.00E-11	2.25	0	0	2.15	-7.90	3.36	-3.96	-3.55	4.62
	Final	2.95E-11	2.25	0	0	3.88	-6.34	5.12	-2.33	-1.91	4.25

Table 10 Calibrated model results and errors

Samples	N_{ET} **(cycles)**	N_{CT} **(cycles) Tanaka**	N_{CT} **(cycles) Xiangqiao**	**error (%) Tanaka**	**error (%) Xiangqiao**
1	293971	305376	305376	3.88	3.88
2	431871	404492	404492	-6.34	-6.34
3	322727	339235	339235	5.12	5.12
4	201827	197122	197122	-2.33	-2.33
5	203206	199315	199315	-1.91	-1.91

in combination with the NASGRO equation, as a tool to analyze the fatigue crack growth under the action of a mixed-mode loading (I + II). By means of numerical simulation, it is possible to obtain precise results of the stress intensity factors and the crack path, while with the NASGRO equation, a good estimation of the number of load cycles is achieved.

The post-processing of the numerical results to calculate the range of the equivalent stress intensity factor in mixed-mode loading (I + II) showed that Tanaka and Xiangqiao criteria resulted in virtually the same values. Since Tanaka criterion has an empirical formulation and Xiangqiao criterion is based on the maximum tangential stress theory, the reasons for the great similarity between their results have not been established. In this sense, it is more practical to use Tanaka criterion for this application, since it only depends on the ranges of the stress intensity factors $\triangle K_{\mathrm{I}}$ and $\triangle K_{\mathrm{II}}$, while Xiangqiao criterion also depends on the crack growth direction θ.

7. Declaration of competing interest

None declared under financial, professional and personal competing interests.

8. Acknowledgments

To the Research Management Direction (DGI) at Pontificia Universidad Católica del Perú (PUCP), for the financial support for this investigation. To the Computer Aided Research Group (INACOM) of Mechanical Engineering Section at PUCP, for providing the hardware and software used in numerical simulations. To the Welding Engineering Institute (INGESOLD) and Materials Laboratory of Engineering Department at PUCP, for providing the equipment and materials used in experimental tests.

References

[1] H. A. Richard, W. Linnig, and K. Henn, "Fatigue crack propagation under combined loading," *Materials Science*, 1991.

[2] S. B. Biner, "Fatigue crack growth studies under mixed-mode loading," *International Journal of Fatigue*, vol. 23, 2001. [Online]. Available: https://doi.org/10.1016/S0142-1123(01)00146-3

[3] S. Seitl and Z. Knésl, "Two parameter fracture mechanics: Fatigue crack behavior under mixed mode conditions," *Engineering Fracture Mechanics*, vol. 75, no. 3-4, February 2008. [Online]. Available: https://doi.org/10.1016/j.engfracmech.2007.04.011

[4] M. Ševčík, P. Hutař, L. Náhlík, and S. Seitl, "The effect of constraint level on a crack path," *Engineering Failure Analysis*, vol. 29, April 2013. [Online]. Available: https://doi.org/10.1016/j.engfailanal.2012.11.011

[5] A. L. L. Silva, A. M. P. de Jesus, J. Xavier, J. A. F. O. Correia, and A. A. Fernandes, "Combined analytical-numerical methodologies for the evaluation of mixed-mode (I + II) fatigue crack growth rates in structural steels," *Engineering Fracture Mechanics*, vol. 185, November 2017. [Online]. Available: https://doi.org/10.1016/j.engfracmech.2017.04.016

[6] Y. Li and G. F. Wang, "Influence of surface tension on mixed-mode cracks," *International Journal of Applied Mechanics*, vol. 7, no. 5, 2015. [Online]. Available: https://doi.org/10.1142/S1758825115500702

[7] K. P. Mróz and Z. Mróz, "On crack path evolution rules," *Engineering Fracture Mechanics*, vol. 77, no. 11, July 2010. [Online]. Available: https://doi.org/10.1016/j.engfracmech.2010.03.038

[8] H. A. Richard, B. Schramm, and N. H. Schirmeisen, "Cracks on mixed mode loading – theories, experiments, simulations," *International Journal of Fatigue*, vol. 62, May 2014. [Online]. Available: https://doi.org/10.1016/j.ijfatigue.2013.06.019

[9] X. Zhang and *et al.*, "Experimental and numerical investigation of fatigue crack growth in the cracked gear tooth," *Fatigue & Fracture of Engineering Materials & Structures*, vol. 40, no. 7, July 2017. [Online]. Available: https://doi.org/10.1111/ffe.12557

[10] G. Vukelic and J. Brnic, "Numerical prediction of fracture behavior for austenitic and martensitic stainless steels," *International Journal of Applied Mechanics*, vol. 9, no. 4, 2017. [Online]. Available: https://doi.org/10.1142/S1758825117500521

[11] M. Schöllmann, M. Fulland, and H. A. Richard, "Development of a new software for adaptive crack growth simulations in 3D structures," *Engineering Fracture Mechanics*, vol. 70, no. 2, January 2003. [Online]. Available: https://doi.org/10.1016/S0013-7944(02)00028-0

[12] H. Pathak, A. Singh, and I. V. Singh, "Fatigue crack growth simulations of 3-D problems using XFEM," *International Journal of Mechanical Sciences*, vol. 76, November 2013. [Online]. Available: https://doi.org/10.1016/j.ijmecsci.2013.09.001

[13] F. Erdogan and G. C. Sih, "On the crack extension in plates under plane loading and transverse shear," *Journal of Basic Engineering*, vol. 85, no. 4, 1963. [Online]. Available: https://doi.org/10.1115/1.3656899

[14] G. C. Sih, "Strain-energy-density factor applied to mixed mode crack problems," *International Journal of Fracture*, vol. 10, pp. 305–321, 1974.

[15] M. A. Hussain, S. L. Pu, and J. Underwood, "Strain energy release rate for a crack under combined mode I and mode II," in *Fracture Analysis: Proceedings of the 1973 National Symposium on Fracture Mechanics Part II*, West Conshohocken, PA, 1974, pp. 2–28.

[16] J. M. Barsom, E. J. Imhof, and S. T. Rolfe, "Fatigue-crack propagation in high yield-strength steels," *Engineering Fracture Mechanics*, vol. 2, no. 4, June 1971. [Online]. Available: https://doi.org/10.1016/0013-7944(71)90016-6

[17] S. K. Putatunda and J. M. Rigsbee, "Effect of specimen size on fatigue crack growth rate in AISI 4340 steel," *Engineering Fracture Mechanics*, vol. 22, no. 2, 1985. [Online]. Available: https://doi.org/10.1016/S0013-7944(85)80034-5

[18] P. C. Paris and F. Erdogan, "A critical analysis of crack propagation laws," *Journal of Basic Engineering*, vol. 85, no. 4, December 1963. [Online]. Available: https://doi.org/10.1115/1.3656900

[19] R. G. Forman, V. Shivakumar, and J. C. Newman, "Fatigue-crack-growth computer program," NASA, Houston, TX, United States, Tech. Rep. MSC-21669, Apr. 1991.

[20] S. Klysz, J. Lisiecki, A. Leski, and T. Bakowski, "Least squares method modification applied to the NASGRO equation," *Journal of Theoretical and Applied Mechanics*, vol. 51, no. 1, pp. 3–13, Jan. 2013.

[21] W. Zhang, Q. Wang, X. Li, and J. He, "A simple fatigue life prediction algorithm using the modified NASGRO equation," *Mathematical Problems in Engineering*, vol. 2016, June 30 2016. [Online]. Available: https://doi.org/10.1155/2016/4298507

[22] B. Moreno, A. Martin, P. Lopez, J. Zapatero, and J. Dominguez, "Estimations of fatigue life and variability under random loading in aluminum Al-2024t351 using strip yield models from NASGRO," *International Journal of Fatigue*, vol. 91, October 2016. [Online]. Available: https://doi.org/10.1016/j.ijfatigue.2015.09.031

[23] J. C. Newman, "A crack opening stress equation for fatigue crack growth," *International Journal of Fracture*, vol. 24, pp. 131–135, 1984.

[24] J. Maierhofer, R. Pippan, and H. P. Gänser, "Modified NASGRO equation for physically short cracks," *International Journal of fatigue*, vol. 59, February 2014. [Online]. Available: https://doi.org/10.1016/j.ijfatigue.2013.08.019

[25] K. Tanaka, "Fatigue crack propagation from a crack inclined to the cyclic tensile axis," *Engineering Fracture Mechanics*, vol. 6, no. 3, October 1974. [Online]. Available: https://doi.org/10.1016/0013-7944(74)90007-1

[26] Y. Xiangqiao, D. Shanyi, and Z. Zehua, "Mixed-mode fatigue crack growth prediction in biaxially stretched sheets," *Engineering Fracture Mechanics*, vol. 43, no. 3, October 1992. [Online]. Available: https://doi.org/10.1016/0013-7944(92)90115-U

[27] J. Weertman, "Rate of growth of fatigue cracks calculated from the theory of infinitesimal dislocations distributed on a plane," *International Journal of Fracture Mechanics*, vol. 2, pp. 460–467, 1966.

[28] R. W. Lardner, "A dislocation model for fatigue crack growth in metals," *Philosophical Magazine*, vol. 17, no. 145, 1968. [Online]. Available: https://doi.org/10.1080/14786436808218181

[29] D. Wang and S. Y. Du, "On the modified fracture criterion of the maximum tangential stress criterion," *J. Harbin Inst. Technol.*, pp. 58–64, 1976.

[30] S. T. Rolfe and J. M. Barsom, *Fracture and fatigue control in structures: applications of fracture mechanics*. New Jersey, USA: Prentice-Hall, 1977.

[31] M. R. Ayatollahi, S. M. J. Razavi, and M. Y. Yahya, "Mixed mode fatigue crack initiation and growth in a CT specimen repaired by stop hole technique," *Engineering Fracture Mechanics*, vol. 145, August 2015. [Online]. Available: https://doi.org/10.1016/j.engfracmech.2015.03.027

[32] D. Ferreño, J. M. Alegre, and J. M. Revilla, "Simulación del efecto de la plastificación en la propagación de fisuras por fatiga en modo mixto," in *XXIII Encuentro del Grupo Español de Fractura*, Albarracín, España, 2006, pp. 275–280.

[33] *Standard Test Methods and Definitions for Mechanical Testing of Steel Products*, ASTM A370, 2013.

[34] *Standard Test Methods for Rockwell Hardness of Metallic Materials 1,2*, ASTM E18, 2014.

[35] *Standard Test Method for Linear-Elastic Plane-Strain Fracture Toughness KIC of Metallic Materials*, ASTM E399, 2013.

[36] *Standard Guide for Preparation of Metallographic Specimens*, ASTM E3, 2017.

[37] *Standard Practice for Microetching Metals and Alloys*, ASTM E407, 2015.

[38] D. R. Berrios and R. Franco, "Análisis experimental y numérico de la trayectoria de propagación de fisuras por fatiga utilizando XFEM," *Inf. Tecnol.*, vol. 29, no. 5, 2018. [Online]. Available: http://dx.doi.org/10.4067/S0718-07642018000500019

[39] M. Stern, E. B. Becker, and R. S. Dunham, "A contour integral computation of mixed-mode stress intensity factors," *International Journal of Fracture*, vol. 12, pp. 359–368, Jun. 1976.

[40] J. F. Yau, S. S. Wang, and H. T. Corten, "A mixed-mode crack analysis of isotropic solids using conservation laws of elasticity," *Journal of Applied Mechanics*, vol. 47, no. 2, June 1980. [Online]. Available: https://doi.org/10.1115/1.3153665

[41] J. P. Pereira and C. A. Duarte, "The contour integral method for loaded cracks," *Communications in Numerical Methods in Engineering*, vol. 22, no. 5, May 2006. [Online]. Available: https://doi.org/10.1002/cnm.824

[42] M. Skorupa, T. Machniewicz, J. Schijve, and A. Skorupa, "Application of the strip-yield model from the NASGRO software to predict fatigue crack growth in aluminium alloys under constant and variable amplitude loading," *Engineering Fracture Mechanics*, vol. 74, no. 3, February 2007. [Online]. Available: https://doi.org/10.1016/j.engfracmech.2006.06.014

[43] B. Moreno, A. Martin, P. Lopez, J. Zapatero, and J. Dominguez, "On the use of NASGRO software to estimate fatigue crack growth under variable amplitude loading in aluminium alloy 2024-T351," *Procedia Engineering*, vol. 101, 2015. [Online]. Available: https://doi.org/10.1016/j.proeng.2015.02.037

[44] B. Cotterell, "Notes on the paths and stability of cracks," *International Journal of Fracture Mechanics*, vol. 2, pp. 526–533, 1966.

[45] L. P. Pook, "Five decades of crack path research," *Engineering Fracture Mechanics*, vol. 77, no. 11, July 2010. [Online]. Available: https://doi.org/10.1016/j.engfracmech.2010.04.010